ELSEVIER

Cement & Concrete Composites 23 (2001) 3–19

Cement & Concrete Composites

www.elsevier.com/locate/cemconcomp

# Improved model for plate-end shear of CFRP strengthened RC beams

Omar Ahmed, Dionys Van Gemert *, Lucie Vandewalle

*Department of Civil Engineering, Katholieke Universiteit Leuven, W. De Croylaan 2, B-3001 Heverlee, Belgium*

Received 27 August 1999; accepted 21 September 2000

**Abstract**

In case of RC members strengthened by means of externally bonded reinforcement, a premature failure can be detected in addition to the conventional modes of failure observed in RC unstrengthened beams. The premature failure occurs mainly due to both shear and normal stresses induced in either the external reinforcement–concrete interface or at the level of steel reinforcement. This research is part of a complete programme aiming to set up design formulae to predict the strength of CFRP strengthened beams, particularly when premature failure through laminates-end shear or concrete cover delamination occurs. Series of RC beams were strengthened with carbon-fiber-reinforced plastic (CFRP) laminates and tested to estimate the extent of the applicability of the formulae proposed by the authors, as well as to study the influence of the layout of the external reinforcement in terms of unsheeted length (the distance between CFRP laminates-end and the nearer support) and cross-sectional area, on the behaviour of strengthened beams. The predictions using the proposed formulae are compared with the obtained experimental results, as well as with the calculated design limit states. The interfacial shear stress and the maximum deflection corresponding to the predicted values at maximum and service loads are also studied. 

*Keywords:* Carbon-fiber-reinforced plastic (CFRP) laminates; Anchorage shear stress; Strengthening; Shear-span; Unsheeted length

## 1. Introduction

Carbon-fiber-reinforced plastic (CFRP) laminates are becoming a powerful technique for strengthening RC beams. The technique intends to enhance the flexural capacity of the original beam. However, when applying the CFRP laminates to the beam, geometrical as well as material discontinuities are introduced into the composite system (beam/adhesive/laminates).

Similarly, as in the steel plate bonding technique, the unsheeted length in the shear zone near the beam supports has an important effect on the general behaviour and strength of the system. Due to higher strength of the laminates, their cross-sectional area is reduced, and therefore the geometrical relation between concrete and laminates is completely different from the one in bonded steel plates.

In steel plate bonding only exceptionally more than one layer of plates are used. However, in CFRP laminates bonding, it is very easy to comprise of multiple laminates and laminate layers with different lengths. The use of different lengths can be applied to alleviate stress concentration at the laminates anchorages [1].

This paper deals with mathematical modelling and prediction of behaviour and strength of CFRP laminates strengthened beams, in particular when failure occurs due to laminates-end shear or concrete cover delamination, taking into account the influence of unsheeted length and the cross-sectional area of CFRP. This paper does not deal with other failure mechanisms like peeling-off of laminates at the laminates ends or at intermediate locations such as large shear or flexural cracks [2].

Tests on a series of RC beams with externally bonded CFRP laminates have been used in this research to confirm the validity of the proposed formulae to be applied in the case of CFRP strengthened beams in both ultimate and design limit states.

* Corresponding author. Fax: +32-016-32 19 76.

*E-mail address:* dionys.vangemert@bwk.kuleuven.ac.be (D. Van Gemert).

0958-9465/01/$ - see front matter 
PII: S0958-9465(00)00051-2

## 2. Mathematical modelling

### 2.1. Shear stress analysis

For a homogeneous beam, Kim and White [3] analysed the shear stress induced over the surface in a horizontal cross-section at the level of the internal bars as well as at that in a vertical cross section. After the formation of flexural cracks, the shear stresses over the surface in a horizontal cross-section do not remain constant but change considerably, see Fig. 1(c). Equilibrium of an element pp′m′n′ (Fig. 1(b)) is considered, with the reinforcement tension force $T$ acting on the flexural crack. The average shear stress $\tau_{avg}$ acting on the horizontal plane pp′ is obtained according to (Eq. (1)). Eq. (1) needs a careful consideration because of the discontinuities caused by cracking and complexities in stress distribution caused by the composite action of steel and concrete. More specific, these discontinuities are caused by the effect of bond between the concrete and the rebar and the effect of the development of arch action.

After the flexural crack n′p′ forms (Fig. 1(b)), bond phenomena lead to highly concentrated shear stresses in the zone above the internal bars, adjacent to the flexural crack (Figs. 1(a), (b) and (d)). In the critical zone, a maximum shear stress is present, with a value of double or more the average stress. Hence, a magnification factor $m_{bond}$ is introduced which, according to Kim, is equal to or more than 2. On the other hand, the neutral axis shifts upward after the occurrence of flexural cracks, (Fig. 2). In the shear-span, the real lever arm tends to be smaller than the one calculated by means of the cracked section analysis. Kim explains this by the fact that when flexural cracks extend, the compressive stress distribution becomes more uniform. Accordingly, the neutral axis shifts downward. This is attributed to the development of arch action. As a result of the reduction of the internal lever arm from $z_0$ to $z_c$ (Fig. 2(a)), the reinforcement force $T$ in the shear-span is consistently higher than the calculated value. Hence, a magnification factor $m_{arch}$ is introduced, which equals the actual internal moment arm length $z_c$ over the calculated moment arm $z_0$. With regard to Kim's

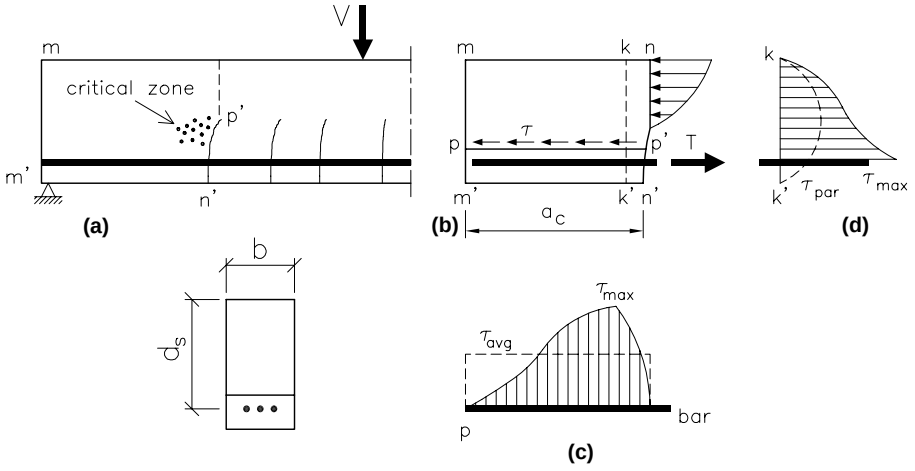


Fig. 1. Shear stress in reinforced concrete beams, Kim and White (1991).

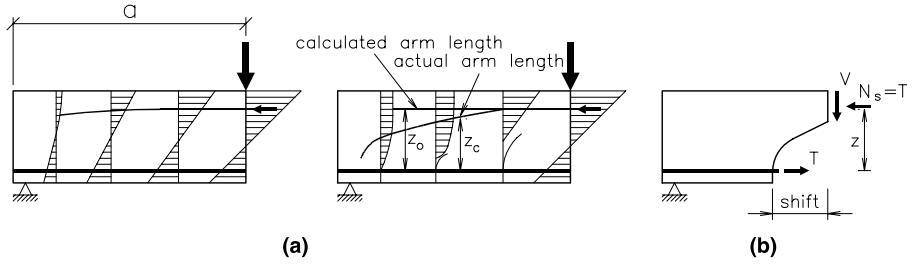


Fig. 2. (a) Reduction of internal moment arm length due to the development of arch action by flexural cracks based on finite-element analysis, before flexural cracking (left) and after flexural cracking (right), Kim and White (1991); (b) shift rule: reinforcement force is dependent on the shear force acting at a distance $z$.

explanation, it is remarked that the increased reinforcement force is normally accounted for by the so-called "shift-rule" in a cross-section. It is calculated with the shear load acting on the concrete compression zone of the cross-section at the tip of the flexural crack (Fig. 2(b)).

On the basis of these considerations Kim and White derived two cracking criteria. The first criterion, (Eq. (2)), describes the flexural shear cracking load, when the shear stress $\tau$ reaches the tensile strength $f_t$ of concrete. Then, a shear crack may initiate at a point in the critical zone in which the magnification factors $m_{arch}$ and $m_{bond}$ only have a meaning after flexural cracking. For a simply supported beam under point loads, the second criterion, (Eq. (3)), describes the shear force as a function of the flexural cracking moment at a section $a_c$ from the support. By equilibrating the two criteria, a probable flexural shear load and a flexural shear crack position $a_c$ emerge. The critical crack position $a_c$ is expressed by Eq. (4).

$$\tau = \frac{T}{ba_c}, \tag{1}$$

$$V_{cr} = \frac{1}{m_{arch}m_{bond}} f_t b z_0, \tag{2}$$

$$V_{cr} = \frac{M_{cr}}{a_c} \tag{3}$$

and

$$a_c = k_3 \left[ \frac{\rho_s (d_s/a)^2}{\left(1-\sqrt{\rho_s}\right)^2} \right]^{1/3} a \tag{4}$$

with $\rho_s$ = reinforcement ratio and $k_3$ = empirical constant.

### 2.2. Modelling analogy according to Jansze [4]

If RC members are partially strengthened by means of externally bonded steel plates, a plate-end shear crack is forced to occur at the plate-end location. Hence, the plate-end position or the unplated length $L$ is analogous to the location of the critical shear crack $a_c$ of Kim and White. This is depicted in Fig. 3. On the left side, the critical crack section of Kim and White is depicted, the right side shows a partially plated beam-end. As a result of the analogy between $a_c$ and $L$, the shear-span $a$ belonging to $a_c$ is analogous to the fictitious shear-span $a_L$ belonging to $L$. When taking this modelling analogy into account, Eq. (4) can be interpreted as Eq. (5).

The fictitious shear-span $a_L$ given by Eq. (5) is used by Jansze as input parameter to compute the shear resistance $\tau_{cum}$ on the basis of MC90[5]-formula (7) [5], where $C_{MC90} = k = 0.18$ (Eq. (10)) in case of ultimate load. Essential is that with this MC90-formula the unstrengthened part is considered, so the effective depth of the internal reinforcement $d_s$ and the internal reinforcement ratio $\rho_s$ have to be taken into account. Kim has used a statistical analysis to determine the constant $k_0$ included in Eq. (4). Also, to satisfy the prediction of the maximum shear load, the formulation has been adjusted by Jansze [4]. Analysis showed that by replacing the constant $k_0$ included in Eq. (5) by the fictitious shear-span-to-depth ratio $a_L/d_s$, a correct agreement was obtained between the plate-end shear loads based on the fictitious shear-span and the experimental and numerical results. Thus, by substituting constant $k_0$ in Eq. (5) with $a_L/d_s$ it can be rewritten into Eq. (6) that objectively expresses the fictitious shear-span $a_L$. Hence, when Eq. (6) is used in combination with the modified MC90 (Eq. (10)) to predict the plate-end shear strength $\tau_{PES}$ of strengthened beams with different unplated lengths [4], the conclusion is drawn that the plate-end shear model is definitely capable of calculating the plate-end shear strength of partially plated members with various cross-sections.

$$L = k_0 \left[ \frac{\rho_s (d_s/a_L)^2}{\left(1-\sqrt{\rho_s}\right)^2} \right]^{1/3} a_L, \tag{5}$$

$$a_L = \sqrt[4]{\frac{\left(1-\sqrt{\rho_s}\right)^2}{\rho_s} d_s L^3}, \tag{6}$$

$$\tau_{cum} = C_{MC90} \sqrt[3]{3\frac{d_s}{a}} \left(1 + \sqrt{\frac{200}{d_s}}\right) \sqrt[3]{100\rho_s f_{cm}} \quad \text{[CEB – FIP MC90]}. \tag{7}$$

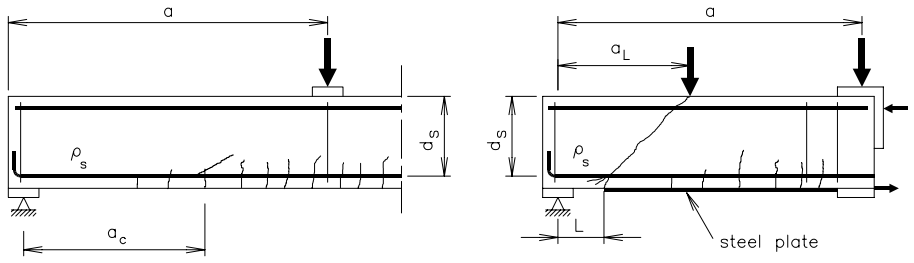


Fig. 3. Location $a_c$ of governing flexural shear crack according to Kim and White (1991); modelling analogy with fictitious shear-span $a_L$ and unplated length $L$ for partially plated member for which plate-end shear crack is analogous to flexural shear crack.

Furthermore, throughout the experiments carried out by Jansze on strengthened beams of different concrete sections as well as throughout various other studies [6,7] on plate-end shear and plate separation, Jansze found that the described plate separation loads showed a lower bound value ($x - 1.64s$) of 0.84 in the case of steel plates and 0.83 for the FRP plates. As a result, a characteristic lower bound of 0.83 times the mean maximum shear load is advised. Then the plate-end shear model should be multiplied by a factor 0.83 for a safe design. As a consequence, the constant $k = 0.18$ in Eq. (10) should be replaced by the design factor $0.83 \times 0.18 = 0.15$. Moreover, the mean value of the concrete cylinder compressive strength should be replaced by the characteristic compressive cylinder strength. Then the design for plate-end shear and plate separation can be obtained according to Eqs. (6) and (10). It is worthwhile to mention that the modified MC90 formula is corresponding to the shear cracking stress as recommended by the MC90 code for reinforced concrete beams. Accordingly, the plate-end shear model is a lower bound model for the maximum shear load and for plate separation by concrete cover rip-off.

### 2.3. Proposed analytical model

The common dominant failure mode of RC beams strengthened with externally bonded CFRP laminates is the premature one, either laminates-end shear or concrete cover delamination. Therefore, the significant parameter affecting the failure behaviour of a strengthened beam is the shear stress in the adhesive layer between the external reinforcement and the concrete $\tau_{tot}$. The critical section locates at the longitudinal laminates-end region (cut-off point), where the shear stress concentration occurs. Such a shear stress is partially due to the variation of bending moment, part $\tau_{SF}$, and the remaining part due to the introduction of forces in the anchoring zones, part $\tau_{anch}$ (anchorage shear stress). The first portion of shear stress has a considerable role in the case of steel plate bonding. On the contrary, that portion of shear stress is considerably smaller in the case of CFRP laminates technique (Fig. 4). This is attributed to the lower stiffness of the externally bonded reinforcement in case of CFRP laminates: the CFRP laminates strength amounts to 7–10 times that of steel plates, and the modulus of elasticity of the CFRP laminates used in the experimental programme is greater than that of steel plates. A much smaller area of laminates is thus normally needed.

Due to the specific shear stress situation mentioned before, and based on Eq. (10), suggested by Jansze, the authors propose modified formulae to predict the load carrying capacity of RC beams strengthened by means of externally bonded CFRP laminates, particularly for those failed due to either laminates-end shear or concrete cover delamination. Therefore, the shear strength $\tau_{PES}$ (PES = plate-end shear) calculated from Eq. (10) will be replaced by $\tau_{FES}$ (FES = fiber-end shear). The authors propose to add the modification $\Delta\tau_{MOD}$ given in Eq. (11) to obtain $\tau_{FES}$ instead of $\tau_{PES}$, (Fig. 5 and Eqs. (8)–(12)). The proposed modified expression relies mainly on adding the difference between the portion of shear stress generated due to shear force in case of substitution of CFRP laminates with steel plates of 550 $N/mm^2$ yield strength (the case of Jansze's study) and that for CFRP laminates, to the shear stress calculated from Eq. (10). Moreover, contribution of the original shear strength of the beam to be strengthened to the obtained strength is taken into account [8]. The second term in Eq. (11) dealing with the influence of the original shear strength is added to the formula presented in the literature [1,9]. This term accounts for an original shear strength $\tau$ ($\tau$ is calculated according to ACI code [10], Eq. (12)) different from that of reference strengthened beams.

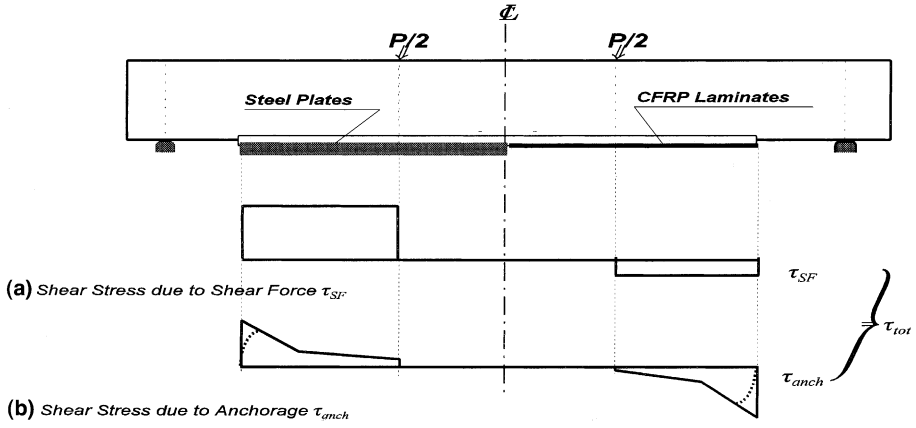


Fig. 4. Shear stresses in the external reinforcement–concrete interface.

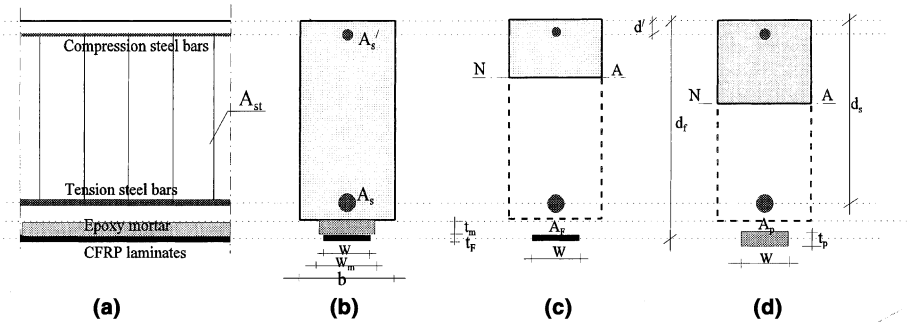


Fig. 5. Details of strengthened beam: (a) longitudinal section; (b) cross-section; (c) cracked cross-section; (d) assumed equivalent cracked cross-section.

The fictitious shear-span $a_L$ calculated according to Eq. (6) may be greater than the true shear-span $a$. A fictitious shear-span $a_L$ larger than the true one $a$ is not logic. In such cases, Jansze proposed to limit $a_L$ to the true value $a$. In our experiments, we found that an imaginary value $a_{LM}$ equal to the average of the calculated fictitious shear-span and the true shear-span should replace the value $a_L$ included in Eq. (10). This adaptation is always applied by the authors.

$$F_{FES} = \tau_{FES}\, bd_s \leqslant F_u, \tag{8}$$

$$\tau_{FES} = \tau_{PES} + \Delta\tau_{MOD}, \tag{9}$$

$$\tau_{PES} = k\sqrt[3]{3\frac{d_s}{a_L}}\left(1+\sqrt{\frac{200}{d_s}}\right)\sqrt[3]{100\rho_s f_c} \quad \text{(Jansze, 1997)} \tag{10}$$

$$\Delta\tau_{MOD} = \tau_{PES}\, bd_s\left(\frac{S_p}{I_p W} - \frac{S_F}{I_F W_m}\right) + m\left(\frac{\tau-\tau_{ref}}{bd_s}\right), \tag{11}$$

$$\tau = \left(0.15776\sqrt{f_c} + \frac{17.2366\rho_s F_u d}{M_u}\right) + 0.9 \times \frac{A_{st} f_{yst}}{sb} \quad \text{[ACI Code]}, \tag{12}$$

where $k, m, \tau_{ref}$ are 0.18, 6188.5 and 4.121 in case of maximum load and are 0.15, 7236.5 and 2.75 in case of design load, $S_F, I_F$ the statical moment of area and moment of inertia of transformed (to concrete) cracked section in case of CFRP, $S_P, I_P$ the statical moment of area and moment of inertia of transformed (to concrete) cracked section in case of replacing CFRP with steel plates, $\rho_s$ the ratio of continuous tension reinforcement, $f_c$ the mean compressive cylinder concrete strength, $W, W_m$ the widths of both CFRP and epoxy mortar, respectively (Fig. 5(b)), $M_u/F_u$ represents the shear-span ($a$), $A_{st}, f_{yst}$ the cross-sectional area and yield strength of shear reinforcement, $s$ the spacing between internal stirrups, $F_u$ is the smaller of either shear capacity or flexural capacity of the strengthened beam ($P = 2F$).

## 3. Outline of experiments

### 3.1. Test programme

Nine RC beams with a rectangular cross-section of 125 mm width and 225 mm height were tested under a two-point loading bending test over a simple span of 1500 mm (shear-span to depth ratio, $a/d$, equals 2.5). These beams were divided into two main groups.

The beams in the first group were designated as AF.0, AF.2, AF.2-1, AF.3 and AF.4. These beams were reinforced with two bottom bars ($A_s$) of 8 mm in diameter and two top bars of 6 mm in diameter plus stirrups of 6 mm in diameter at a spacing ($s$) of 71 mm (Fig. 6). The first beam AF.0 was tested in its original condition as a control one. The rest of the beams were strengthened with two layers of longitudinal CFRP laminates ($A_F$) of 75 mm width and variable lengths (Table 1 and Fig. 7).

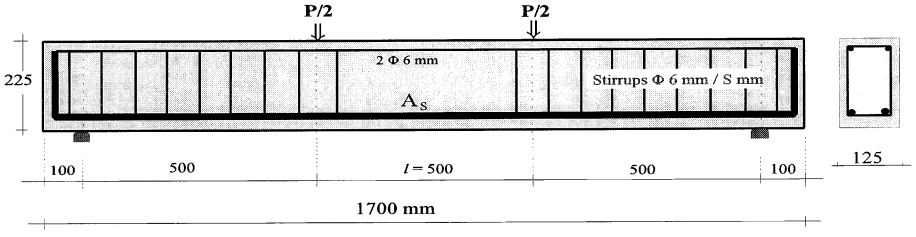


Fig. 6. Details of tested beam reinforcements.

Table 1
Details and data of tested beams

| Beam no. | Internal reinforcement | | $f_c$ (MPa) | Epoxy mortar | | CFRP laminates | | Notice |
|---|---|---|---|---|---|---|---|---|
| | $A_s$ | $s$ (mm) | | $L'$ (mm) | $W_m$ (mm) | $A_F$ (mm$^2$) | $L$ (mm) | |
| AF.0 | | | 41.0 | – | – | – | – | Ref. |
| AF.2 | | | 41.0 | 200 | 125 | 25.05 | 200 | |
| AF.2-1 | 2Φ8 mm | 71 | 41.0 | 150 | 125 | 25.05 | 150 | |
| AF.3 | | | 41.0 | 100 | 125 | 25.05 | 100 | |
| AF.4 | | | 41.0 | 50 | 125 | 25.05 | 50 | |
| CF.3-0 | | 71 | 43.0 | – | – | – | – | Ref. |
| DF.1 | | | 42.0 | 32 | 125 | 12.53 | 50 | |
| DF.2 | 3Φ8 mm | 100 | 42.0 | 43 | 125 | 25.05 | 50 | |
| DF.4 | | | 40.5 | 50 | 125 | 50.10 | 50 | |

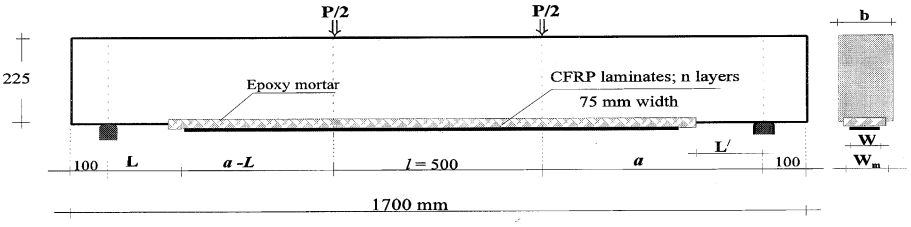


Fig. 7. Details and arrangements of bonded laminates for tested beams.

These two layers were bonded symmetrically onto the bottom concrete surface of the beam. The main parameter taken into account in this group is the distance between the cut-off point and the nearer support, the so-called unsheeted length ($L$).

The beams in the second group were designated as CF.3-0, DF.1, DF.2 and DF.4. These beams were reinforced with three tension bars of 8 mm in diameter ($A_s$) and two top bars of 6 mm in diameter plus stirrups of 6 mm in diameter at a spacing ($s$) (Fig. 6 and Table 1). The first beam CF.3-0 was the control one. Beams DF.1, DF.2 and DF.4 were strengthened with one, two and four layers of longitudinal CFRP laminates, respectively. Both the length and width of longitudinal CFRP laminates are the same and equal to 1400 and 75 mm, respectively (unsheeted length to shear-span ratio $L/a = 0.10$) as shown in Fig. 3 and Table 1. For this group of beams, the main parameter is the cross-sectional area of the CFRP laminates.

### 3.2. Materials

All beams were made using a normal strength coarse aggregate concrete of 16 mm maximum nominal size, 350 kg/m$^3$ Portland cement (CEM I, 42.5) and a w/c of 0.55. This concrete mix achieved mean compressive strength, surface tensile strength (pull-off strength) and Young's modulus of 45.0, 2.85 and 30 000 MPa, respectively. The mean compressive strengths ($f_c$) on the cylinder after 42 days (time of testing) are listed in Table 1 for the different tested beams.

Ribbed bars (BE 500) of 8 mm in diameter were used for tension reinforcement and of 6 mm for both compression and web reinforcements (stirrups). Both yield and ultimate strengths as well as Young's modulus for each diameter are mentioned in Table 2.

The external reinforcement was a CFRP laminate [11]. Such a CFRP is available in rolled laminate of 0.167 mm effective thickness, 500 mm width and 100 m length. The effective thickness gives the section of the fibers in each single ply. The ultimate strength (rupture strength) and Young's modulus of the CFRP laminate are given in Table 2.

An epoxy mortar layer of 2.5–3.5 mm thickness was applied to the different strengthened beams as a

Table 2
Properties of used reinforcements

| Properties (N/mm$^2$) | Internal reinforcement | | External reinforcement (CFRP laminate) |
|---|---|---|---|
| | Φ6 (mm) | Φ8 (mm) | |
| Yield strength | 553 | 568 | – |
| Ultimate strength | 613 | 654 | 3500 |
| Young's modulus | 195 000 | 185 000 | 240 000 |

substratum to the CFRP laminates. This epoxy mortar is almost completely cured within a period of 24 h after application. Then the compressive, bending and tensile strengths as well as Young's modulus of this epoxy mortar amount to 80, 20, 6.5 and 7200 N/mm$^2$, respectively. The resin used for the completion of CFRP impregnation was a special epoxy resin, which was developed for an easy impregnation of the laminate.

### 3.3. Preparation of test specimens

The beams were prepared for bonding after a period of 3 weeks from casting. The concrete surfaces where the epoxy mortar layer was applied were roughened using sand-blasting technique. Before the application of the epoxy mortar, the roughened surfaces were cleaned by brushing and compressed air to remove any attached fine materials.

## 4. Experimental results and discussion

The influence of both the unsheeted length and the amount of externally bonded CFRP laminates on the behaviour of tested beams are discussed. Table 3 gives the following elements:

| | |
|---|---|
| $P_{cr}$ | cracking load |
| $P_{gr}$ | growth load (load at which the end laminates shear crack initiates) |
| $P_{max}$ | ultimate rupture load |
| $\delta_{cr}$ | mid-span deflection at first cracking |
| $\delta_{max}$ | maximum mid-span deflection (the deflection corresponding to the maximum load) |
| $\tau_{tot}$ | maximum interfacial shear stress induced along the bonded length |
| $\tau_{SF}$ | interfacial shear stress due to shear force. |

### 4.1. Failure behaviour

The first crack initiated as a flexural one at the middle third (region of constant moment) in case of both reference and strengthened beams. The mode of failure was a flexural one for the reference beams. However, it changed from laminates-end shear to concrete cover delamination as the unsheeted length decreased (Fig. 8). The results recorded by Oehlers [2,12,13] concerning the failure mode confirm the obtained results. When considering the cross-sectional area of the CFRP laminates, the failure mode changed from a flexural one (yielding of internal steel bars and rupture of CFRP laminate) to concrete cover delamination to laminates-end shear as the amount of CFRP increased (Fig. 9). The obtained results showed a similar trend to that observed by Tumialan [14]. Furthermore, it is worth noting that the growth load was affected considerably by the variation of the unsheeted length: it increased as the unsheeted length decreased (Table 3). On the contrary, it was found that the growth load was not influenced significantly by the variation of the amount of the externally bonded CFRP laminates.

### 4.2. Maximum loads and load–deflection diagrams

The used strengthening technique enhanced the cracking load. The obtained enhancement was not affected by the variation of the unsheeted length. However, it was influenced reasonably by the variation of the amount of externally bonded CFRP laminates. When considering the load carrying capacity $P_{max}$, the strengthened beams showed a considerable enhancement in comparison to that of the corresponding reference beam. The unsheeted length showed a significant effect on the load carrying capacity (Fig. 18). On the contrary, the gained strength did not correspond to the increase in the amount of CFRP, particularly at a higher

Table 3
Results of tested beams

| Beam no. | Loads (kN) | | | Shear stress (MPa) | | Deflection (mm) | | Mode of failure |
|---|---|---|---|---|---|---|---|---|
| | $P_{cr}$ | $P_{gr}$ | $P_{max}$ | $\tau_{SF}$ | $\tau_{tot}$ | $\delta_{cr}$ | $\delta_{max}$ | |
| AF.0 | 20.0 | – | 55.0 | – | – | 0.77 | 10.60 | Flexure/ref. |
| AF.2 | 25.0 | 55.0 | 83.0 | 0.47 | 1.17 | 1.06 | 8.44 | Laminates-end shear |
| AF.2-1 | 25.0 | 60.0 | 85.7 | 0.51 | 1.21 | 1.01 | 10.16 | Laminates-end shear |
| AF.3 | 25.0 | 65.0 | 96.5 | 0.54 | 1.45 | 1.08 | 13.16 | Laminates-end shear |
| AF.4 | 25.0 | 105.0 | 111.0 | 0.63 | 2.23 | 0.87 | 14.63 | Concrete cover |
| CF.3-0 | 20.0 | – | 75.0 | – | – | 0.64 | 11.16 | Flexure/ref. |
| DF.1 | 25.0 | 105.0 | 118.0 | 0.28 | >1.72 | 0.78 | 20.80 | Flexure[a] |
| DF.2 | 30.0 | 100.0 | 120.0 | 0.51 | 1.84 | 1.01 | 13.60 | Concrete cover delamination |
| DF.4 | 28.0 | 100.0 | 125.0 | 0.87 | 1.98 | 0.91 | 10.00 | Laminates-end shear |

[a] Flexure due to yielding of internal steel and rupture of externally bonded CFRP laminates.

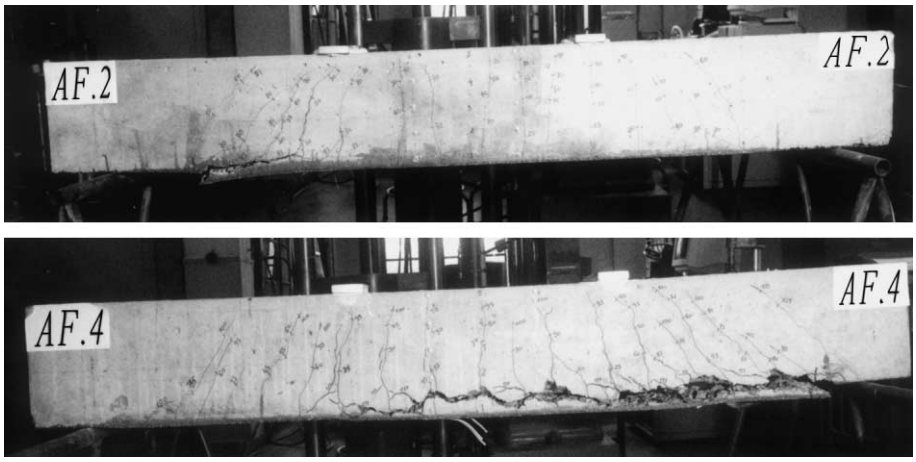


Fig. 8. Crack pattern of beams AF.2 and AF.4 ($L = 200$ and 50 mm).

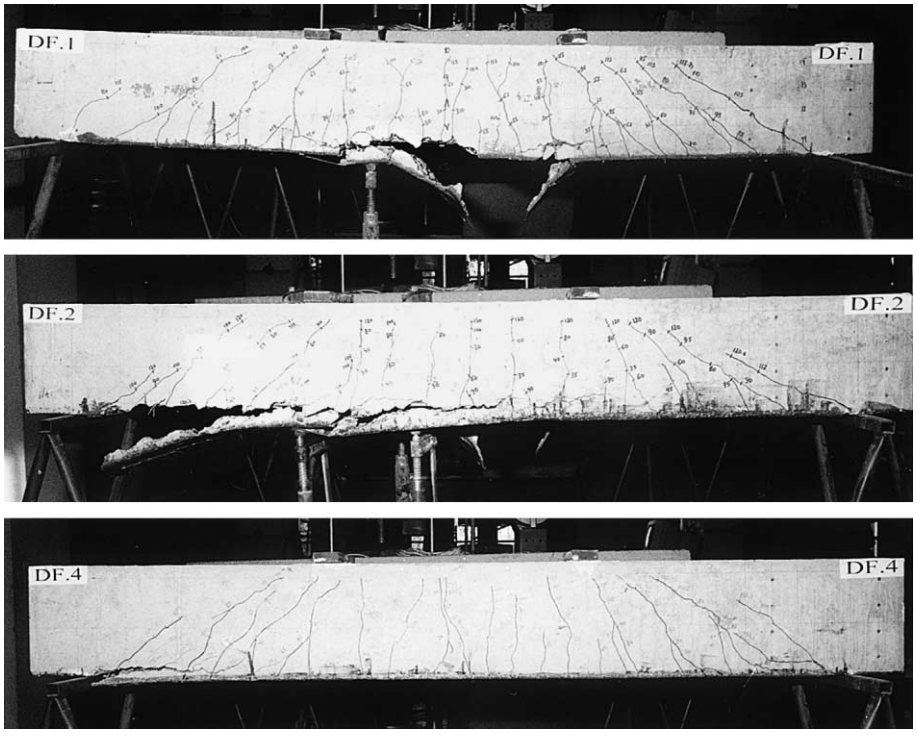


Fig. 9. Crack pattern of beams DF.1, DF.2 and DF.4 ($A_F = 12.53$, 25.05 and 50.1 mm$^2$).

strengthening ratio ($A_F/A_s$), (Fig. 19). The load carrying capacity of the strengthened beam increased as the strengthening ratio increased. However, for strengthening ratios higher than about 8%, a very slight enhancement was observed in the gained strength as the strengthening ratio increased. This does not mean that the value of 8% of the experiments is the common optimum strengthening ratio. The optimum value relies mainly on different other parameters such as the original shear strength, the original flexural strength, the concrete strength and the shear-span to depth ratio of the member to be strengthened [8,15–17]. When considering the maximum load, the strengthened beams showed 1.51, 1.56, 1.75 and 2.02 times the load of the corresponding reference beam for unsheeted length of 200, 150, 100, 50 mm, respectively. On the other hand, the strengthened beams showed 1.57, 1.61 and 1.67 times that of the corresponding reference beam for strengthening ratio ($A_F/A_s$) of 8.05%, 16.1% and 32.2%, respectively. The studies of Tumialan [14] and Kachlakev [18] confirm the obtained results well.

The relation between the total applied load and the measured mid-span deflection is illustrated in Figs. 10 and 11 for tested beams with different unsheeted lengths

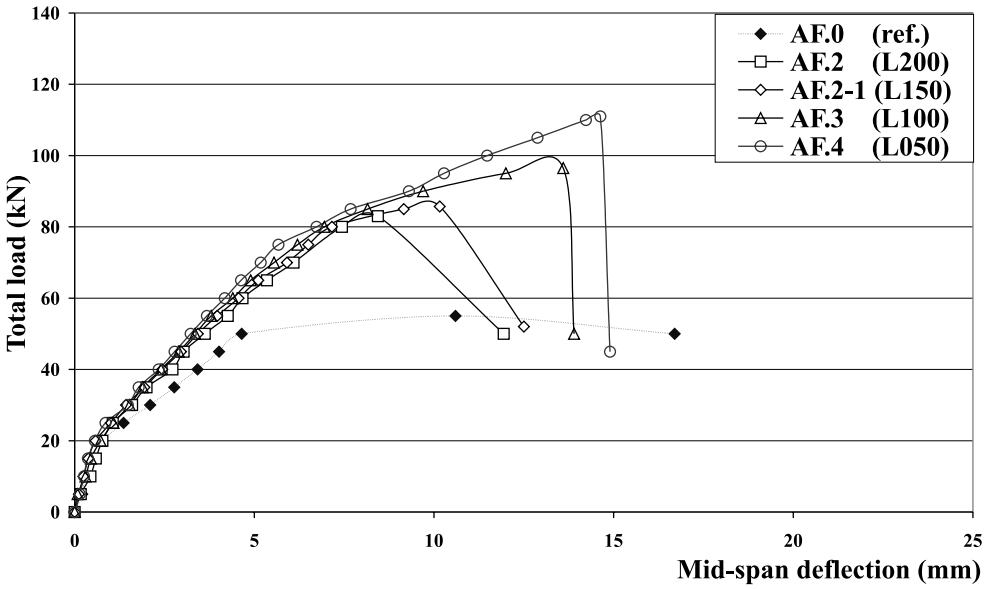


Fig. 10. Load mid-span deflection for beams of different unsheeted lengths.

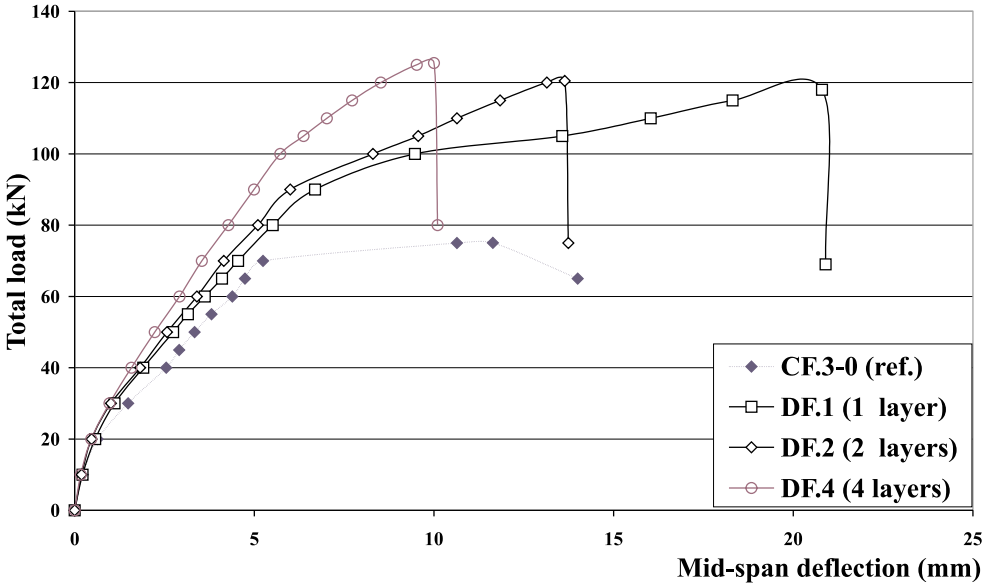


Fig. 11. Load mid-span deflection for beams of different cross-sectional areas of CFRP laminates.

and different amounts of CFRP laminates, respectively. Through these figures it is obvious that, for the same level of loading, the strengthened beams showed a smaller mid-span deflection than that of the corresponding reference beams, particularly after cracking. Before cracking, the used strengthening technique showed no significant influence. On the other side, when considering the relative load (the ratio of the applied load to the maximum load) the strengthened beams showed a greater deflection than that of the corresponding reference beams at the same relative load. The unsheeted length has a slight influence on the mid-span deflection, particularly at lower loading levels. Contrarily to this, a reasonable influence on the bending stiffness emerged due to the variation of the amount of externally bonded CFRP laminates regardless of the loading level. This is attributed to the active contribution of the amount of external longitudinal reinforcement to the overall bending stiffness of the strengthened beam.

### 4.3. Interfacial shear stresses

The shear stress evolution ($\tau$) between the external reinforcement and concrete along the bonded length was derived from the normal stresses of CFRP laminates ($\sigma$) according to Eq. (13), in which $i$ and $i-1$ denote the subsequent cross-sections. The difference between the stresses generated in the subsequent CFRP laminates cross-sections is transmitted to the concrete by shear stresses.

$$\tau_{(i)} = \frac{\sigma_{(i)} t_{f(i)} - \sigma_{(i-1)} t_{f(i-1)}}{\Delta x_{(i)}}. \tag{13}$$

For the various unsheeted lengths as well as for the various amounts of externally bonded CFRP laminates, the shear stress distribution was plotted along the bonded length for different levels of loading as shown in Figs. 12–15. At the CFRP laminates-end region, at the same level of loading, the shear stress decreased as the unsheeted length decreased. Such a laminates-end shear

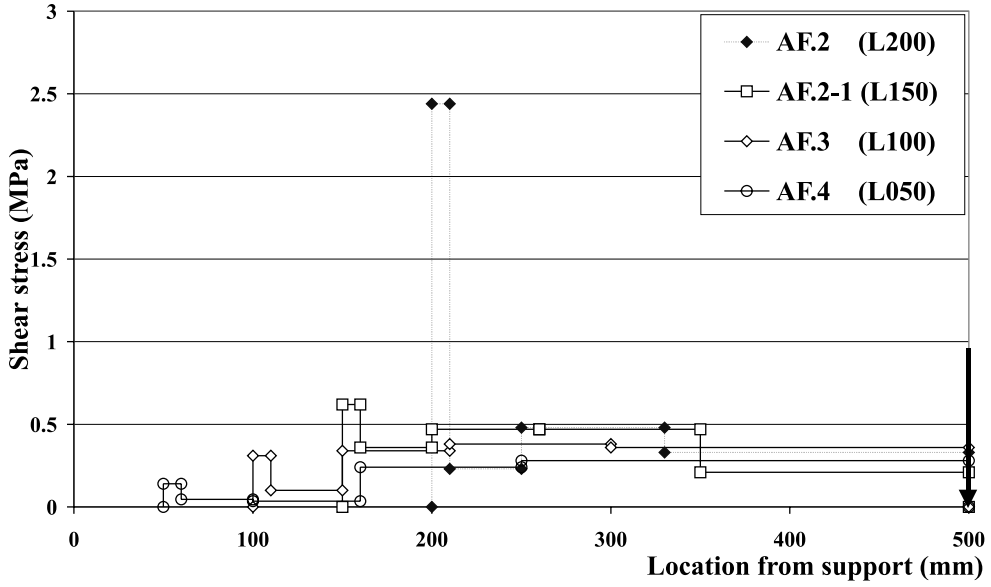


Fig. 12. Shear stresses along the bonded CFRP laminates for the different unsheeted lengths (at $P = 50$ kN).

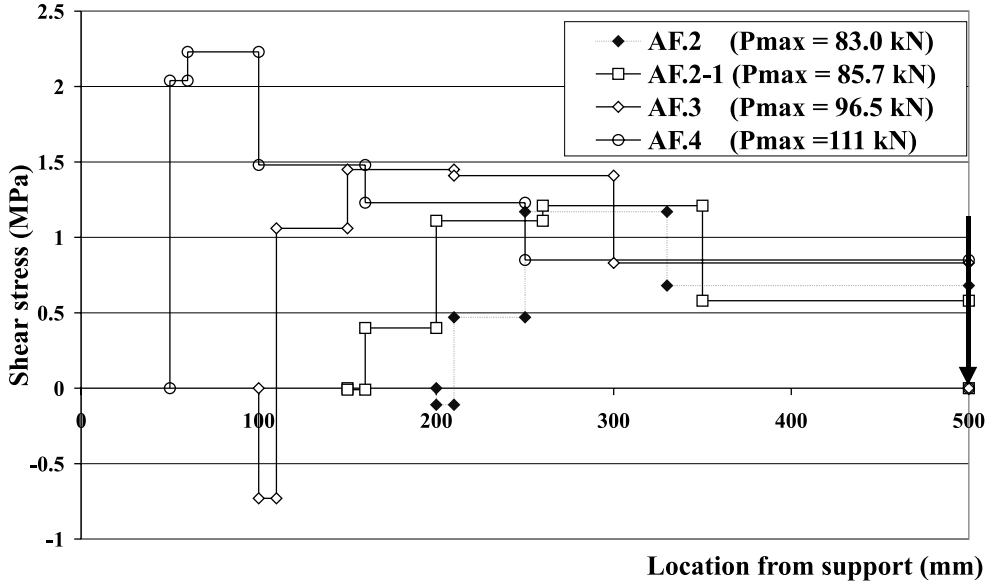


Fig. 13. Shear stresses along the bonded CFRP laminates for the different unsheeted lengths (at the maximum load $P_{max}$).

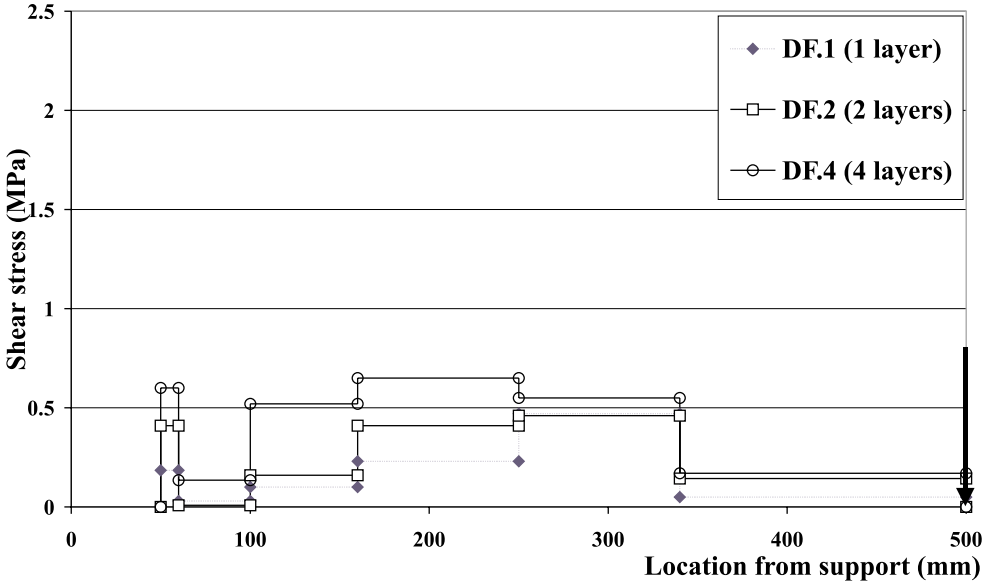


Fig. 14. Shear stresses along the bonded CFRP laminates for the different strengthening ratios (at $P = 70$ kN).

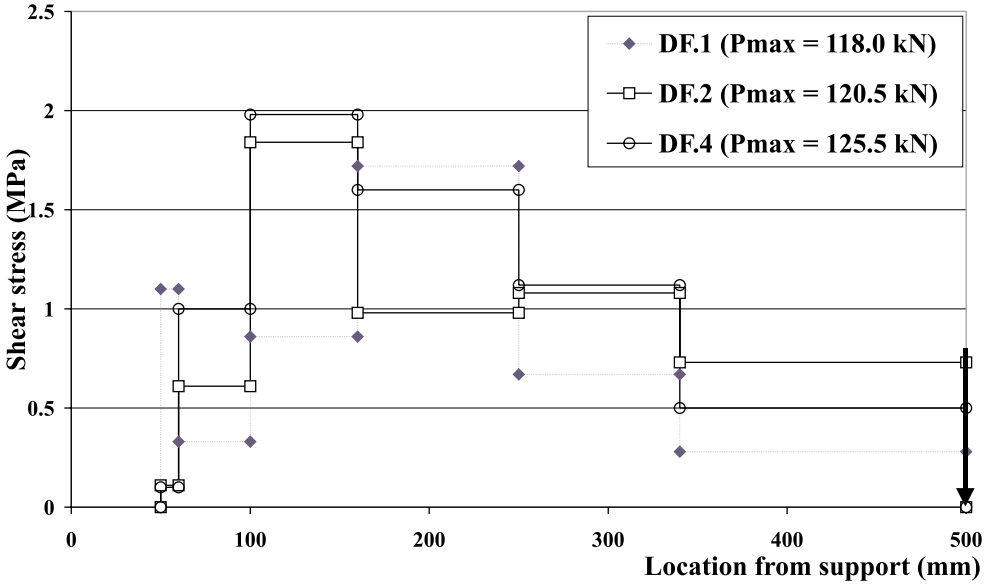


Fig. 15. Shear stresses along the bonded CFRP laminates for the different strengthening ratios (at the maximum load $P_{max}$).

stress plays a major role in the initiation and propagation of the laminates-end shear crack which is normally considered the major crack in case of strengthened beams. The total drop in the shear stress induced at the laminates-end region, just before failure, increased as the unsheeted length increased. Through Fig. 13 and Table 3 it can be observed that the value of maximum shear stress generated at the external reinforcement–concrete interface along the bonded length enhanced considerably as the unsheeted length decreased. This is due to the fact that the concentration and widths of both shear and flexural shear cracks formed at the laminates-end region increased as the unsheeted length increased. These formed cracks weaken the surface tensile strength of the concrete.

In case of beams with different strengthening ratios $A_F/A_s$ ($A_s$ is constant) and at the same level of loading, the shear stress generated at the CFRP laminates-end region increased as the cross-sectional areas of CFRP laminates increased (Fig. 14). The total drop in shear stress induced at the laminates-end region, just before failure, increased as the cross-sectional area of CFRP

laminates increased. Contrarily to that of unsheeted length, the cross-sectional areas of bonded CFRP laminates showed a slight influence on the value of maximum shear stress generated along the bonded length just before failure (Fig. 15 and Table 3).

## 5. Evaluation of the proposed formulae

### 5.1. Maximum load

The predicted load carrying capacity of the strengthened beams obtained according to both the analytical model ($P_{pr}$) proposed by the authors and Jansze's equation ($P_{pr.J}$) was calculated. Also, the maximum flexural capacity for the different tested beams was calculated according to Eurocode 2 [19]. Two values could be obtained according to the proposed analytical model, $P_{pr.a}$ and $P_{pr.b}$. The first value $P_{pr.a}$ is obtained when applying the unsheeted length $L$ to calculate the fictitious shear-span $a_L$. Yet, the second one $P_{pr.b}$ is obtained when applying the unstrengthened length $L'$, the distance between the edge of the epoxy mortar layer and the nearer support (clearance of the layer of the epoxy mortar is taken into account), instead of the unsheeted length $L$ to calculate the fictitious shear-span, (Fig. 7). Herewith, the mathematical model takes into account that the end-laminate shear crack (major crack corresponding to $P_{gr}$) starts at the end of the epoxy mortar layer, and not at the end of the laminate. Fig. 16 shows the ideal case with a major crack which initiated at the end of bonded longitudinal laminates and Fig. 17 shows the case with a major shear crack which initiated at the end of the epoxy mortar layer.

The comparison between the predicted load carrying capacity and that obtained experimentally is illustrated in Figs. 18, 19 and Table 4. The calculated results obtained according to the proposed formulae show a much better approach to the observed values in comparison with those obtained according to the existing literature [4], particularly when the clearance of the epoxy mortar layer is taken into account.

### 5.2. Design load and serviceability limit state

The proposed equation is modified in case of a design procedure for both laminates-end shear and concrete cover delamination. Moreover, limitations of the proposed formulae accommodate the conventional failure modes, shear one and flexural one. The ultimate limit state (ULS) design method may be used in these two cases. A good design not only takes into account the ULS, but it also guarantees a ductile behaviour to allow for a stress distribution.

In some particular cases, the strengthened beams showed a ductile behaviour, e.g. beams of higher shear-span to depth ratio ($a/d > 2.5$) [17] and those provided with adequate end anchorage [1]. The results of the various previous studies on RC beams strengthened by means of externally bonded reinforcements proved that the failure response of the member and the bonded external reinforcement were characterised as brittle. Accordingly, when one should design these brittle failure modes, a lower bound approach of the maximum load carrying capacity is recognized. The safety against fail-


Fig. 16. Major shear crack at the end of bonded laminates.

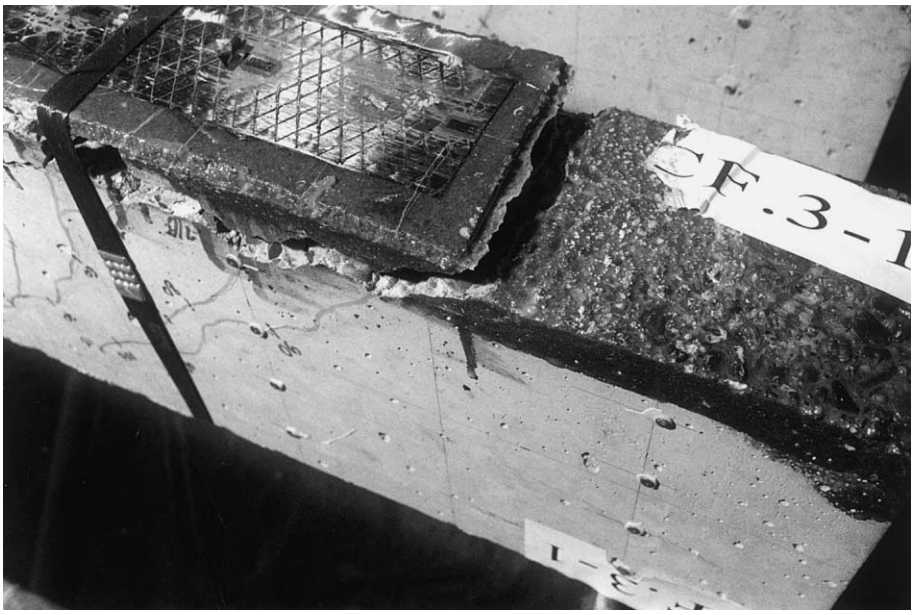


Fig. 17. Major shear crack at the end of epoxy mortar layer.

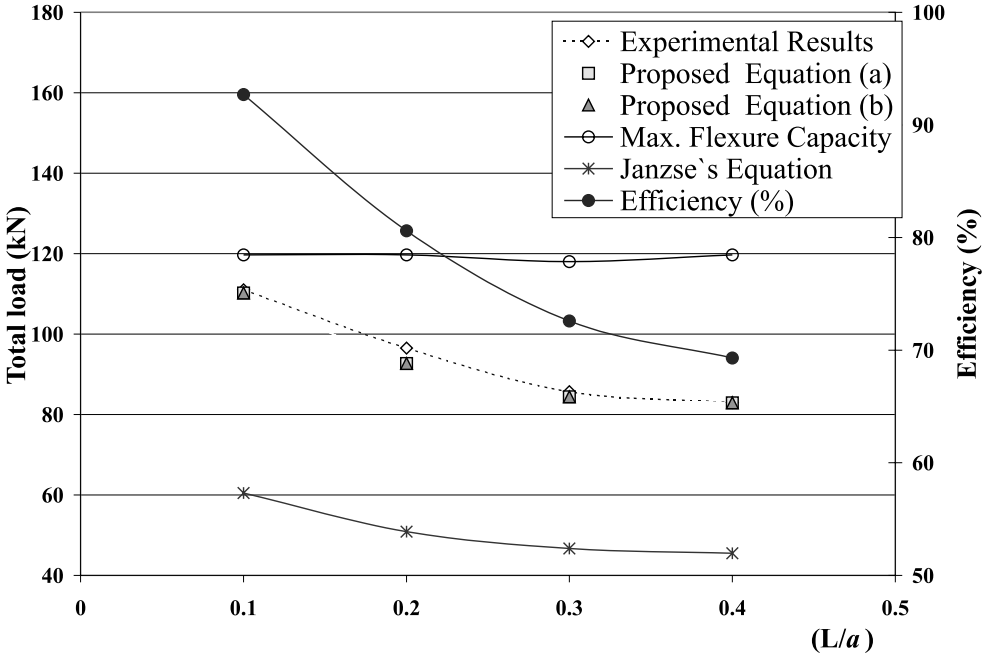


Fig. 18. The predicted results in comparison with that obtained experimentally for the different unsheeted length to shear-span ratios ($L/a$).

ure is expressed as the ultimate limit resistance load $P_{max}$ over the serviceability limit load $P_S$. According to the codes, this safety factor should be taken generally 1:0.6 or nearly 1.70.

The predicted design load $P_d$ was calculated using the proposed equation, taking into account that the mean compressive strength $f_c$ will be replaced by the characteristic compressive strength $f_{ck}$. Also, strength reduction coefficients [20] for both steel and concrete ($\gamma_s$ and $\gamma_c$) of 1.15 and 1.50, respectively, should be taken into account in both Eqs. (10) and (12). The design load was evaluated according to the load carrying capacity of the tested beams. Consequently, it is worth noting that, when considering the design limit state related to the resistance load, the different tested beams fulfilled the required limits. The ultimate limit resistance load over the serviceability limit load ($P_{max}/P_s$) ranged from 1.83 to 2.13.

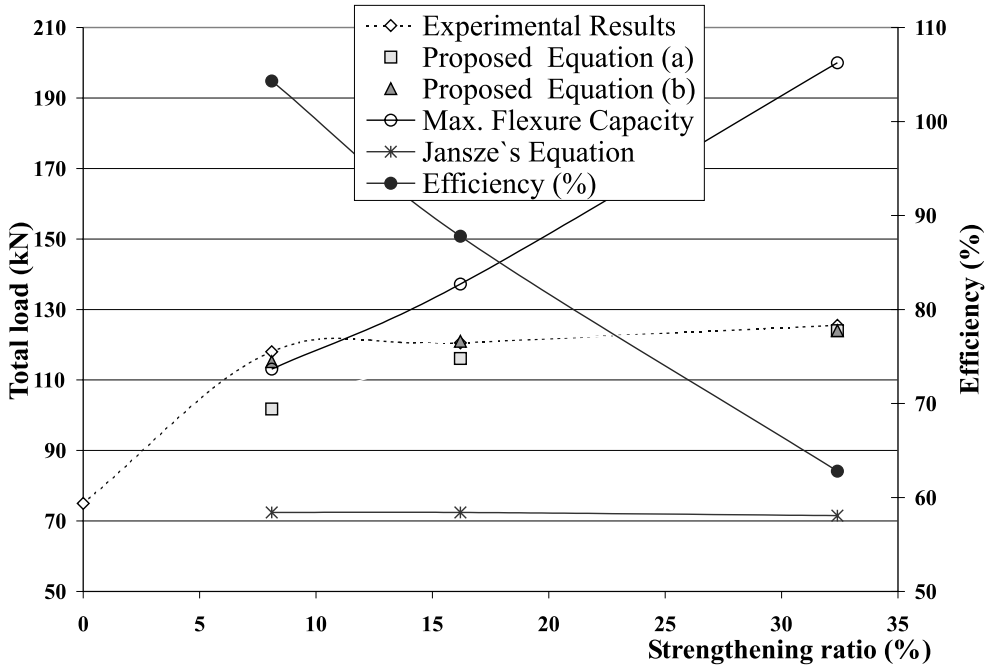


Fig. 19. The predicted results in comparison with that obtained experimentally for the different strengthening ratios ($A_F/A_s$).

Table 4
Predicted results

| Beam no. | $A_F/A_s$ (%) | $L/a$ | Exp. max. load $P_{max}$ (kN) | Predicted results (kN) | | | | Deflection | |
|---|---|---|---|---|---|---|---|---|---|
| | | | | Maximum load | | Design load | | Exp. results | Predicted results |
| | | | | $P_{pr.a}$ (kN) | $P_{pr.b}$ (kN) | $P_{d.a}$ (kN) | $P_{d.b}$ (kN) | $\delta_s$ (mm) | $\delta_{p.s}$ (mm) |
| AF.0 | – | – | 55.0 | – | – | – | – | 1.80[a] | 1.29[a] |
| AF.2 | 24.3 | 0.4 | 83.0 | 83.0 | 83.0 | 61.8 | 61.8 | 2.95 | 2.76 |
| AF.2-1[b] | 24.3 | 0.3 | 85.7 | 84.5 | 84.5 | 64.3 | 64.3 | 3.1 | 3.02 |
| AF.3 | 24.3 | 0.2 | 96.5 | 92.7 | 92.7 | 69.1 | 69.1 | 3.25 | 3.25 |
| AF.4 | 24.3 | 0.1 | 111.0 | 110.2 | 110.2 | 82.1 | 82.1 | 4.13 | 4.11 |
| CF.3-0 | – | – | 75.0 | – | – | – | – | 2.60[c] | 2.32[c] |
| DF.1 | 8.1 | 0.1 | 118.0 | 101.8 | 115.2 | 77.7 | 87.9 | 3.97 | 3.89 |
| DF.2 | 16.2 | 0.1 | 120.5 | 116.1 | 121.0 | 88.6 | 92.4 | 4.18 | 3.76 |
| DF.4 | 32.4 | 0.1 | 125.5 | 124.0 | 124.0 | 94.3 | 94.3 | 3.37 | 3.30 |

[a] Deflection corresponding to a design load of 39.1 kN.
[b] $d = 195$ mm.
[c] Deflection corresponding to a design load of 57.40 kN.

The safety factor could also be defined as the ultimate deformation $\delta_u$ over the deformation corresponding to the service load $\delta_s$. In case of the tested beams, when considering this serviceability limit state, the ultimate deformation over the deformation corresponding to the service load ranged from 2.97 to 5.24. The obtained results approach reasonably the value of the corresponding reference beams, particularly in case of beams of smaller unsheeted length and adequate strengthening ratio as well as when the modification dealing with the safety against sudden failure is considered (Eq. (17)). In most cases the final failure mode of the strengthened beams remains brittle. However, when defining ductility as the deflection at failure divided by the deflection at the yielding of steel bars [21], the strengthened beams showed a reasonable ductility in comparison to that of the corresponding reference beams.

Based on the formulations suggested by ACI Code [20] in case of conventional RC beams, the maximum deflection can be given by Eq. (14), taking into account

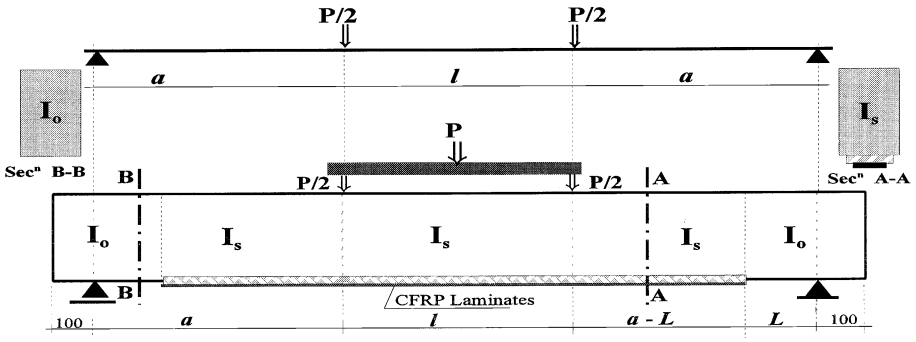


Fig. 20. Load configuration and details of tested beams.

the change in the stiffness along the beam length due to partial strengthening (Eq. (15), Fig. 20). The maximum deflection corresponding to the service load, $\delta_{p.s}$, was calculated and compared with the obtained observed value, $\delta_s$. The used modified equation showed a considerable approach to the true values up to a loading level of 80% of the maximum load (Table 4).

$$\delta = \frac{1}{EI_{ee}}\left(\frac{Pa^3}{6} + \frac{Pa^2 l}{4} + \frac{Pal^2}{16}\right), \tag{14}$$

$$I_{ee} = \frac{I_{es}\left([a + (l/2)]^3 - [l/2]^3 - L^3\right) + I_{eo}L^3}{[a + (l/2)]^3 - [l/2]^3}, \tag{15}$$

$$I_e = k^3 I_g + (1 - k^3) I_{cr}, \tag{16}$$

where

$$k = \frac{M_{cr}}{M_a}, \quad M_{cr} = \frac{f_t I_g}{y_t}, \quad f_t = 1.4 f_c^{0.44},$$

$I_e$ the effective moment of inertia, $I_{cr}$ the moment of inertia of the cracked section, $I_{ee}$ the equivalent effective moment of inertia of the partial strengthened beam, $I_{es}$ the effective moment of inertia of the cracked section in strengthened zone, $I_{eo}$ the effective moment of inertia of the cracked section in unstrengthened zone, $I_g$ the gross moment of inertia of the cross-section (both external and internal reinforcements are neglected), $M_{cr}$ the cracking bending moment, $M_a$ the applied bending moment, $y_t$ the lever arm of the tension concrete fibre and $f_c, f_t$ are the compressive and tensile concrete strengths.

Based on the previous and current studies as well as on the practical and laboratory experience, the authors suggest another safety factor that deals with the initiation of the laminates-end shear crack which is normally a major crack: the design load should be smaller than the growth load [22,23]. Experiments showed that after the initiation of the laminates-end shear crack, the

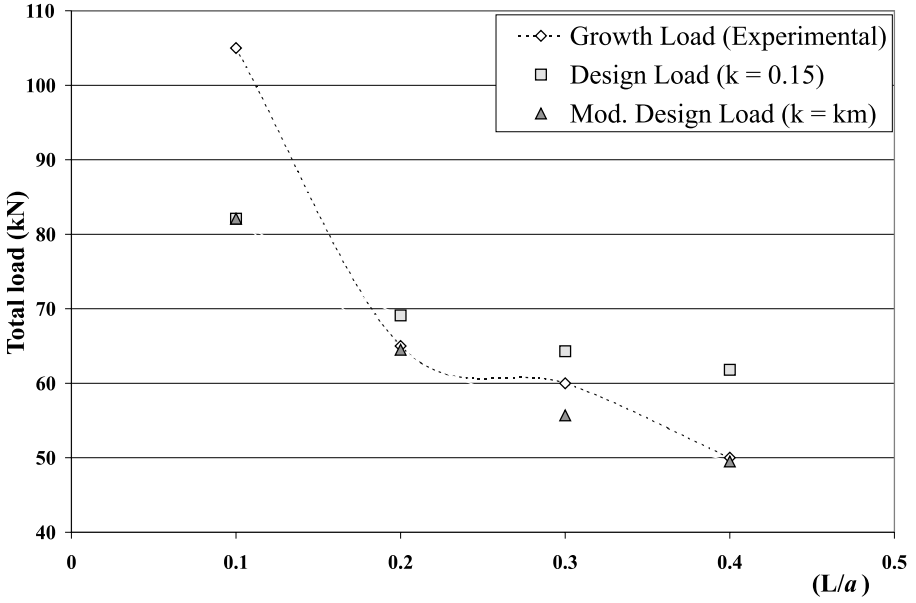


Fig. 21. The predicted design loads in comparison with the growth load for the different unsheeted length to shear-span ratios ($L/a$).

failure could occur suddenly depending considerably upon both the unsheeted length and the original shear strength. Hence, it is worth noting that in case of smaller unsheeted length, $L/a \preceq 0.10$, such a design limit is always fulfilled. On the contrary, for $L/a > 0.10$ this design limit is normally not fulfilled. Therefore, the authors suggest a modified expression for the factor $k$ included in Eq. (10) to obtain the modified design load $P_{d.m}$ as follows:

$$k = k_m = 0.15 - 0.10[L/a - 0.10] \preceq 0.15 \quad \text{for } 0.40 \succeq L/a \succeq 0.10. \tag{17}$$

Fig. 21 illustrates the values of the design load calculated according to the proposed formula, before and after applying the modification in the constant $k$, $k_m$, in comparison to the obtained growth load for the different unsheeted lengths. Throughout this figure it is obvious that the proposed modification added an extra safety factor against premature failure.

## 6. Conclusions

1. The technique of externally bonded CFRP laminates achieves considerable strengthening efficiency, particularly in case of smaller unsheeted length and adequate strengthening ratios.
2. The experiments allowed to set up a modified analytical model for the load carrying capacity of CFRP strengthened RC beams, in case of ultimate and design states, particularly for beams failed due to laminates-end shear or concrete cover delamination. The correspondence between experiments and predicted values is superior to the predictions by formulae available in the literature. The modification takes into account the specific shear stress situation at the laminates-end zone. Furthermore, the influence of the original shear strength $\tau$ is taken into account.
3. The maximum shear stress generated at the external laminates–concrete interface is not only influenced by the surface tensile strength (pull-off strength) as some of the existing literature mentioned but also by a variation of the unsheeted length: it approaches the concrete surface tensile strength as the unsheeted length decreases. However, a slight effect on the induced shear strength was observed due to variation in the cross-sectional area of the externally bonded CFRP laminates.
4. Based on the safety factor related to growth load, the experiments allowed to set up a modified expression for the constant $k$ included in the proposed formula for the prediction of design load: $k = k_m = 0.15 - 0.10(L/a - 0.10)$ for $0.40 \succeq L/a \succeq 0.10$.

## References


[1] Van Gemert D, Ahmed O, Brosens K. Anchoring of externally bonded CFRP reinforcement. In: International Congress "Creating with Concrete", 1999; Dundee, Scotland.

[2] Oehlers DJ. Premature failure of externally plated reinforced concrete beams. J Struct Eng 1990;116(4):978–95.

[3] Kim W, White RN. Initiation of shear cracking in reinforced concrete beams with no web reinforcement. ACI Struct J 1991;88(3):301–8.

[4] Jansze W. Strengthening of RC members in bending by externally bonded steel plates. PhD Thesis, Delft University of Technology, Delft, 1997.

[5] CEB-FIP Modelcode 1990.

[6] Oehlers DJ. Discussion on Roberts and Haji-Kazemi. Proc Inst Civ Eng Part 2 1992;87:651–63.

[7] Van Gemert D, Van den Bosch M. Dimensionering van gelijmde wapeningen bij op buiging belaste elementen. Tijdschrift der Openbare Werken van België, Nr 1, 1982.

[8] Ahmed O, Van Gemert D. Shear behaviour of RC beams strengthened by longitudinal CFRP laminates. In: Proceedings of the Sixth International Conference 'Modern Building Materials, Structures and Techniques', May 1999; Vilnius, Lithuania, vol. Π, p. 5–11.

[9] Ahmed O, Van Gemert D. Enhancement of R.C. beams by means of externally bonded CFRP laminates. In: Eighth International Colloquium on Structural and Geotechnical Engineering, December 1998; Cairo, Egypt.

[10] ACI Manual of Concrete Practise, 1992. Building Code Requirements for Reinforced Concrete (ACI 318-89), p. 137–47.

[11] Mitsubishi Chemical Corporation. Replark System, Design Guideline, 1995; Tokyo, Japan.

[12] Oehlers DJ, Morton JP. Discussion on Roberts and Haji-Kazemi. Proc Inst Civ Eng Part 2, 1989;87:651–63.

[13] Oehlers DJ. Reinforced concrete beams with plates glued to their soffits. J Struct Eng 1992;118(8):2023–38.

[14] Tumialan G, Serra P, Nanni A. Belarbi A. Concrete cover delamination in R.C. beams strengthened with CFRP sheets. In: Fourth International Symposium Fiber Reinforced Polymer Reinforcement for R.C. Structures, October 1999; Baltimore, USA, p. 725–36.

[15] Ahmed O, Van Gemert D. Influence of grade of concrete on the behaviour of CFRP strengthened beams. In: Proceedings of the Fifth International WTA-Colloquium on Materials Science and Restoration, November 1999; Esslingen, Germany, vol. V, p. 1195–207.

[16] Ahmed O, Van Gemert D. Behaviour of RC Beams Strengthened in Bending by CFRP Laminates. In: Proceedings of the Eighth International Conference Structural Faults + Repair, July 1999; London, UK, p. 141.

[17] Ahmed O, Van Gemert D. Influence of shear-span to depth ratio on the efficiency of CFRP laminates strengthening technique. In: Proceedings of the ACUN- 2 International Composites Meeting "Composites in the Transportation Industry", February 2000; Sydney, Australia, 2000.

[18] Kachlakev DI, Barnes WA. Flexural and shear performance of concrete beams strengthened with FRP laminates. In: Fourth International Symposium "FRPR for R.C. Structures", October 1999; Baltimore, USA, p. 959–72.

[19] Eurocode 2 (1992) ENV 1992-1-1:1991.

[20] ACI Committee 318, Building code requirements for reinforced concrete and commentary, ACI 318-89/ACI 318R-89, American Concrete Institute, Farmigton Hills, MI, 1989; p. 353.

[21] Swamy N, Mukhopadhyaya P, Lynsdale C. Ductility consideration in using GFRP sheets to strengthen and upgrade structures.

In: Third International Symposium on Non-metalic (FRP) Reinforcement for Concrete Structure, 1997; Sapporo, Japan, vol. 1, p. 637–44.

[22] Van Gemert D. Special design aspects of adhesive bonding plates. In: Swamy N, Gaul R, editors. ACI SP 165 repair and strengthening of concrete members with adhesive bonded plates, 1996. p. 25–42.

[23] Jin HH, Kypros P, Peter W. CFRP Plate Strengthening of RC Beams. In: Seventh International Conference on Structural Faults and Repair, 1997; Edinburgh, UK, vol. 2, p. 119–26.